DESIGN AND ANALYSIS OF BIDIRECTIONAL DC-DC CONVERTER FOR PHOTO VOLTAIC SYSTEM WITH ENERGY STORAGE

MUKKALA VENKATA SIVA NAGA RAJU
M.Tech, ST.MARY'S GROUP OF INSTITUTIONS GUNTUR CHEBROLU
S M GAVASKAR MEDABALIMI
Assistant professor, ST.MARY'S GROUP OF INSTITUTIONS GUNTUR CHEBROLU

Abstract-This paper proposes a new isolated three-port bidirectional dc–dc converter. It contains an inductor–capacitor–inductor (LCL)-resonant circuit to achieve zero-current switching (ZCS) for the main switch. A new isolated three-port bidirectional dc–dc converter for simultaneous power management of multiple energy sources is proposed in this paper. The proposed converter has the advantage of using the least number of switches and soft switching for the main switch, which is realized by using an inductor–capacitor–inductor (LCL)-resonant circuit. The converter is capable of interfacing sources of different voltage–current characteristics with a load and/or a dc micro grid. The proposed converter is constructed for simultaneous power management of a photovoltaic (PV) panel, a rechargeable battery, and a load. Simulation results show that the proposed converter is capable of maximum power point tracking control for the PV panel, when there is solar radiation, and controlling the charge and discharge of the battery, when there is surplus energy and power deficiency with respect to the load, respectively. By using the simulation results we can analyze the proposed method.

Index Terms—Battery, bidirectional dc–dc converter, isolated converter, multiport converter, photovoltaic (PV), soft switching, zero-current switching (ZCS)

INTRODUCTION

A multiport dc- dc converter has the advantage of using less number of components, lower cost ,high power density and high efficiency. Multiport converters are of 2 types viz; non- isolated and isolated topologies. nonisolated multiport converters are used for low voltage regulation ratio whereas isolated multiport converters are used for high voltage regulation ratio, usually isolated converter with transformer is used. To integrate multiple dc energy sources of different types to a power grid, multiple independent dc–dc converters are commonly used to step up the time-variant low-level source voltages to a constant high-level voltage that is required by a grid-tie inverter.

The multiport converter topologies can be classified into two categories: non-isolated and isolated topologies [3]. Non-isolated multiport converters are usually used in the applications where a low voltage regulation ratio is required [4], [5]. In contrast, in the applications requiring a high voltage regulation ratio, isolated converters, which contain a transformer, are preferred [6]–[8].

In this paper, the two ports on the LVS are connected to a PV panel and a battery. To simplify the analysis, the proposed converter is analyzed by two separate converters: one is a single-switch LCL-resonant converter[9], and the other is the battery-related buck and boost converter consisting ofL2, S2, andS3. The proposed converter is applied for simultaneous power management of a photovoltaic (PV) system with a battery in this paper. The PV system and the battery are connected to the unidirectional port and the bidirectional port of the converter, respectively. The proposed converter is applied for simultaneous power management of a photovoltaic (PV) system with a battery in this paper. The PV system and the battery are connected to the unidirectional port and the bidirectional port of the converter, respectively.

This paper proposes a new isolated three-port bidirectional dc–dc converter. It contains an inductor–capacitor–inductor (LCL)-resonant circuit to achieve zero-current switching (ZCS) for the main switch. A three-port topology has been proposed by adding one middle branch to the traditional half-bridge converter [16], [17]. It uses less controllable power switches than the half-bridge topology and can achieve zero voltage switching for all main switches.

Compared with the converter using five controllable switches, the proposed converter only use three switches; moreover, when using the same renewable energy source to charge a battery, the nominal voltage of the battery connected to the proposed converter can be higher than that connected to the converter.

TOPOLOGY AND OPERATING PRINCIPLE OF THE PROPOSED CONVERTER

A. Topology of the Proposed Converter

The circuit diagram of the proposed converter is shown in Fig. 1, which consists of a low-voltage-side (LVS) circuit and a high-voltage-side (HVS) circuit connected by a high-frequency transformer.

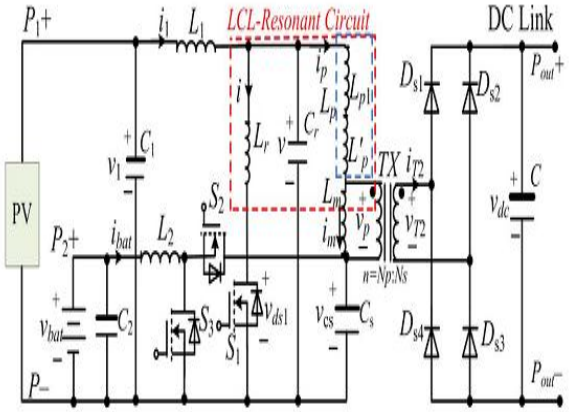

Fig. 1. Proposed isolated three-port bidirectional dc–dc converter for a PV and battery system.

The LVS consists of two ports, an energy storage capacitor Cs, the primary winding of the transformer, and an LCL-resonant circuit consisting of two inductors Lr and Lp and a capacitor Cr, where Lp includes the added inductance Lp1 and the leakage inductance of the transformer L p .The HVS consists of the secondary winding of the transformer and a full-bridge rectifier implemented with the diodesDs1~Ds4.

The transformer's turn ratio is defined as: n=Np/Ns, where Np and Ns represent the numbers of turns of the primary and secondary windings, respectively. Among the switches,S1 is called the main switch because it not only controls the power generated by the source connected to Port 1 (P1) but also changes the direction of the current flowing through the transformer.

B. Single-Switch LCL-Resonant Converter for PV Panel

In a switching period, the voltages across C1 and Cs can be taken as constant values. Particularly, in the steady state, VCs=V1, where V1is the output voltage of the PV panel. The converter has seven operating modes depending on the states of the switchS1 and the resonant circuit.

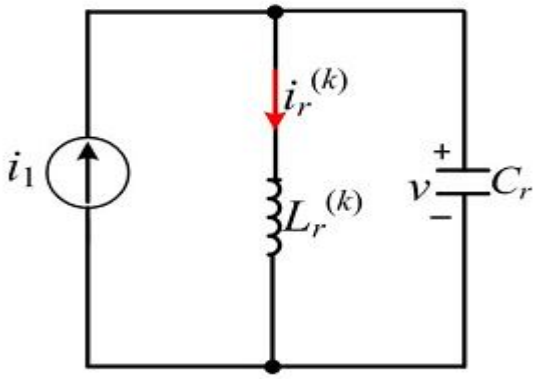

Fig. 2. Equivalent resonant circuit.

Fig. 2 shows the equivalent resonant circuit in different modes. The differential equations of the resonant circuit in Mode k (k=1,...,7)are

$$\begin{cases} v = L_r^{(k)} \cdot \frac{di_r^{(k)}}{dt} \\ i_1 = C_r \cdot \frac{dv}{dt} + i_r^{(k)} \end{cases} \quad (1)$$

Where v represents the voltage of the capacitor Cr; L (k) r and i (k) r represent the equivalent resonant inductance and the current through the equivalent resonant inductor in the kth (k=1,...,7) operating mode, respectively. Then, v can be solved from (1) and has the following form:

$$v(t) = A^{(k)} \cos\left[\left[\omega^{(k)}(t - t_k)\right] + B^{(k)} \sin\left[\omega^{(k)}(t - t_k)\right] + V^{(k)}\right] \quad (2)$$

Where

$$\omega^{(k)} = \frac{1}{\sqrt{L_r^{(k)} \cdot C_r}} \quad (3)$$

is the resonant frequency in Mode k; V (k) is the particular solution of (1) in Mode k, and A(k) and B(k) are coefficients, which can be expressed as follows:

$$A^{(k)} = v(t_k) - V^{(k)} \quad (4)$$

$$B^{(k)} = \frac{I_1 - i_p(t_k) - i(t_k)}{\omega^{(k)} \cdot C_r} \quad (5)$$

Where v(tk), I1, ip(tk), and i(tk)represent the voltage across Cr and the currents ofL1(i1can be viewed as a constant value I1because of a largeL1),Lp, and Lr at time tk, respectively. Equations (4) and (5) indicate that only ω (k) and V (k) are required to determine the parameters of (2).

The steady-state waveforms and equivalent circuits of the seven operating modes of the converter are shown in Figs. 3 and 4, respectively. To facilitate the explanation of the converter operation, define VT=n·Vdc the equivalent output voltage of the converter referred to the primary side of the transformer.

Mode 1—t∈[t1,t2](see Fig. 3): Prior to Mode 1,S1is off; the currents through Lr and Lp are zero and a positive value ofI1, respectively, i.e., i(t1)=0, ip(t1)=I1. When S1is on, as shown in Fig. 4(a), Lr and Lp resonate with Cr, the current of the inductor Lr increases, and the voltage of the capacitor Cr decreases.

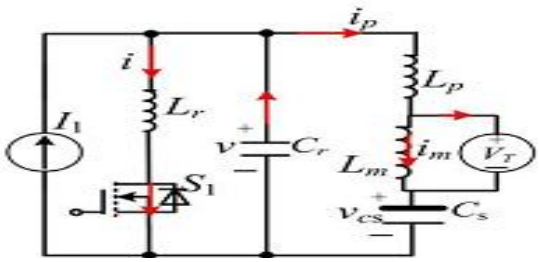

Fig. 4. Equivalent circuits for different operating modes. (a) Mode 1:S1is on,i>0,andvp=VT

Due to the existence of Lr, the current through the switch S1increases slowly, so that the switch is turned on under a low-di/dt condition. The resonant frequency and the particular solution in this mode can be expressed as follows:

$$\omega^{(1)} = \frac{1}{\sqrt{(L_r/L_p).C_r}} \qquad (6)$$

$$V^{(1)} = \frac{L_r}{L_r+L_p}.(V_1 + V_T) \qquad (7)$$

Where // represents that Lr and Lp are connected in parallel. In this mode, the current im through the primary magnetizing inductance Lm increases; the current iT2 through the secondary side of the transformer is positive, which indicates the conduction of theDs1andDs3. At the end of Mode 1,ip(t2)=im(t2), I achieves its maximum value Imax, iT(t2)=0,v(t2)=0, and vp changes its polarity from positive to negative.

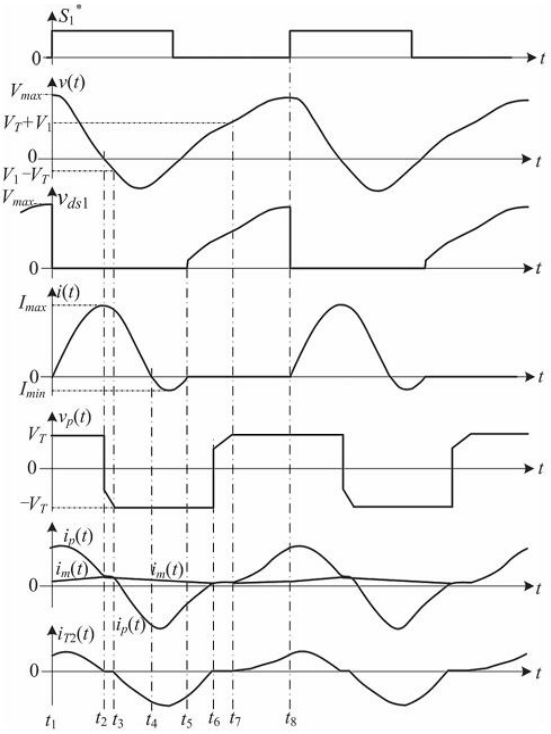

Fig. 3. Steady-state waveforms of the proposed converter.

Mode 2—t∈[t2,t3]: During whichS1 is on, i(t)>0, ip(t)=im(t), and Ds1−Ds4are reverse biased, such that iT= 0. As shown in Fig. 4(b), Lm, Lp, and Lr resonate with Cr. Since LmLp, LmLr, then

$$\omega^{(2)} = 1/\sqrt{[[L_p + L_m]//L_r.\ C_r} \approx 1/\sqrt{L_r.C_r]} \qquad (8)$$

$$V^{(2)} = \frac{L_r}{L_r+L_p+L_m}.V \approx \frac{L_r}{L_m}.V_1 \qquad (9)$$

At the end of Mode 2,vp(t3)=−VT,v(t3)=V1−VT, and the diodesDs2andDs4begin to conduct.

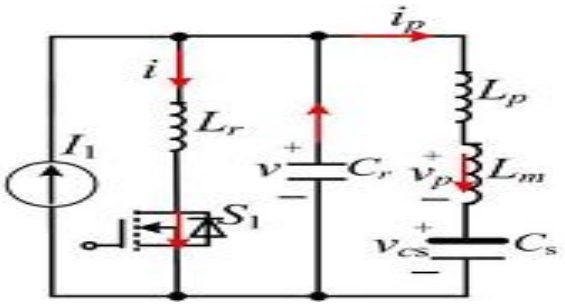

Fig. 4. Equivalent circuits for different operating modes. (b) Mode 2:S1is on,i>0,andip=im.

Mode 3—t∈[t3,t4]: During whichS1 is on, i(t)>0, vp(t)=−VT, and iT2<0. As shown in Fig. 4(c), Lr and Lp resonate with Cr; the energy stored in Lr is released to charge the capacitor Cr; vp is clamped to −VT; and iT2is negative, which indicates the conduction ofDs2andDs4. Compared to Mode 1, the only difference in the equivalent circuit in this mode is the sign of vp. Thus, ω (3) =ω (1) , and

$$V^{(3)} = \frac{L_r}{L_r+L_p}.(V_1 - V_T) \qquad (10)$$

This mode terminates at timet4 when the current of Lr decreases to zero, i.e., i(t4)=0.

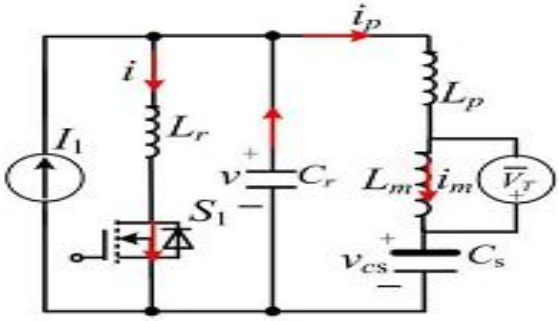

Fig. 4. Equivalent circuits for different operating modes. (c) Mode 3:S1 is on,i>0,andvp=−VT.

Mode 4—t∈[t4,t5]: During whichS1 is on, i(t)<0, vp(t)=−VT, iT2<0, and Ds2andDs4conduct. As shown in Fig. 4(d), a negative current flows through the internal diode of the switchS1; the gate signal can be removed to turn off the switch, e.g., at timet5, under the ZCS condition.

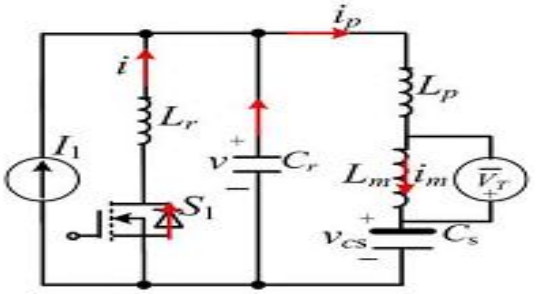

Fig. 4. Equivalent circuits for different operating modes. (d) Mode 4: S1is being turned off ,i<0,andvp=−VT.

The circuit equations are the same as those in Mode 3. Thus, ω (4) =ω (1) , V (4) =V (3) . At the end of Mode 4, i(t5)=0, and the voltage across the switchS1is the same as that across the capacitor Cr, i.e.,vds1(t5)=v.

Mode 5—t∈[t5,t6]: During whichS1is off, i(t)=0,vp= −VT, andiT2<0. As shown in Fig. 4(e),Lr and the switchS1 can be neglected in the circuit. The inductor Lp resonates with Cr, and the direction of ip changes from negative to positive. The following can be obtained:

$$\omega^{(5)} = 1/\sqrt{L_p . C_r} \quad (11)$$

$$V^{(5)} = V_1 - V_T \quad (12)$$

At the end of Mode 5,ip(t6)=im(t6), iT2(t6)=0, and vp changes its polarity from negative to positive.

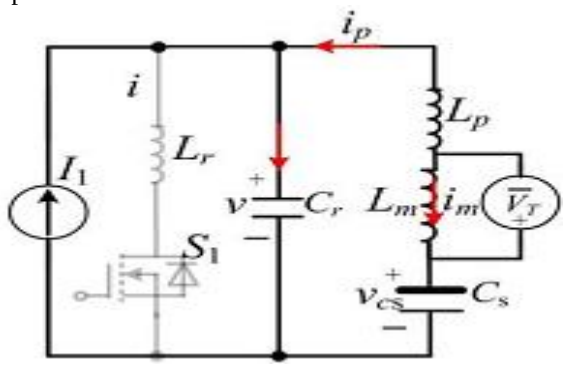

Fig. 4. Equivalent circuits for different operating modes. (e) Mode 5: S1is off,i=0, vp=−VT.

Mode 6—t∈[t6,t7]: During whichS1 is off, i(t)=0, ip(t)=im(t), and Ds1−Ds4 are reverse biased, such that iT2=0. As shown in Fig. 4(f), Lm and Lp resonate with Cr, and Cr is charged. The following can be obtained:

$$\omega_6 = \frac{1}{\sqrt{L_p+L_m}.C_r \approx 1/\sqrt{L_m.C_r}} \quad (13)$$

$$V^{(6)} = V_1 \quad (14)$$

At timet7, v(t7)=V1+VTandvp(t7)=VT

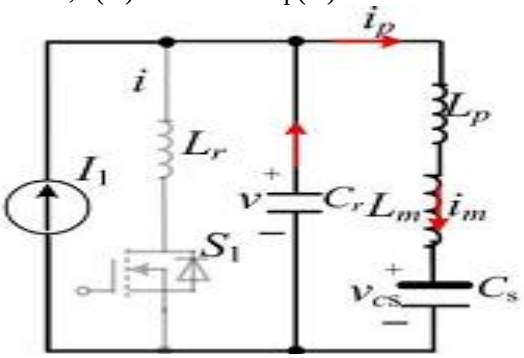

Fig. 4. Equivalent circuits for different operating modes. (f) Mode 6: S1is off,i=0, andip=im. (g) Mode 7:S1is off,i=0,andvp=VT.

Mode 7:t∈[t7,t8], during which S1 is off, i(t)=0, vp(t)=VT, and Ds1andDs3conduct. As shown in Fig. 4(g), Lp resonates with Cr, the circuit equations are the same as those in Mode 5 except the sign of vp, then ω (7) =ω (5) , and

$$V^{(7)} = V_1 + V_T$$

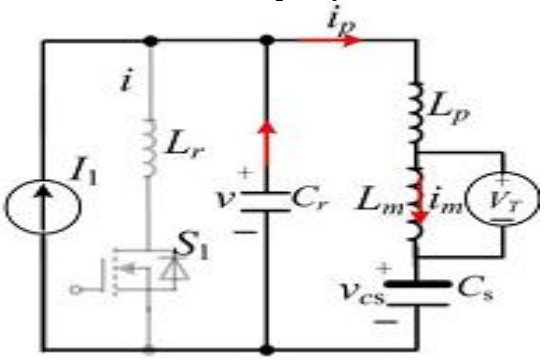

Fig. 4. Equivalent circuits for different operating modes. (g) Mode 7:S1is off,i=0,andvp=VT.

OnceS1is turned on at timet8, Mode 7 switches to Mode 1. There are five inductancesL1, L2, Lr, Lp1, and Lm in the proposed converter that needs to be properly designed. Lm is designed based on the following critical inductance Lmc[19]:

$$L_{mc} = \frac{V_T.T}{4.I_{m.pk}} \quad (16)$$

Where T is the switching period of the switch S1; Im,pk is the peak current through the magnetizing inductor. In this paper, the root-mean-square (RMS) value of the magnetizing current is designed to be 2% of the RMS value of ip. Then, Lm is designed to be larger than Lmc. Once the transformer is designed, the leakage inductance L p of the transformer can be measured.

Given the load resistance RL and the transformer's turn ratio n, the quality factor Q of this LCL-resonant converter can be calculated as follows [20]:

$$Q = \frac{8.n^2.R_L}{\pi^2.Z} \quad (17)$$

Where Z is the characteristic impedance of the resonant circuit

C. Buck and Boost Converter for Battery

The buck and boost converter consists of the inductorL2, switches S2 andS3, and capacitor Cs. When the generated solar power is larger than the power required by the load,S3 is inactive and S2 is switched on to form the buck converter. Then, the surplus energy generated from the PV panel is stored in the battery. In contrast, when the generated solar power is less than the power required by the load, S2 is switched off and S3 is switched on to form the boost converter. The battery is discharged to Cs to provide the deficient energy required by the load.

POWER MANAGEMENT OF THE PROPOSED CONTROLLER

Two controllers are needed to manage the power in the LVS. Their objectives are to regulate the output dc-link voltage to a constant value and

manage the power for the two sources, respectively. According to the availability of the solar power, there are three working scenarios of the converter, as illustrated in Fig. 5.

A. Three Working Scenarios

Scenario 1 (p1≥pout): the available solar power is more than the load demand. As shown in Fig. 5(a), the PV converter works in the MPPT mode; the battery is charged so that the dc-link voltage is controlled at a constant value.

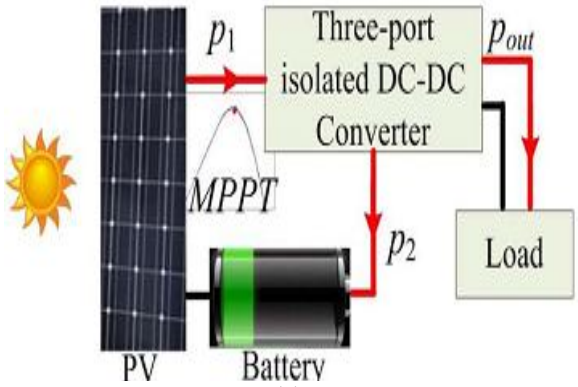

(a)

Fig. 5. Three working scenarios of the converter (the arrows show the directions of energy flow). (a) Scenario 1 (p1>pout): PV works in MPPT mode and the battery works in charge mode to absorb the surplus solar energy

Scenario 2 (0<p1<pout): there is solar radiation, but the solar power is not sufficient to supply the load. As shown in Fig. 5(b), the PV panel is controlled in the MPPT mode by the MPPT algorithm described later. On the other hand, the deficient power is supplied by the battery, which is discharged by the boost converter, so that the dc-link voltage can be maintained at a constant value.

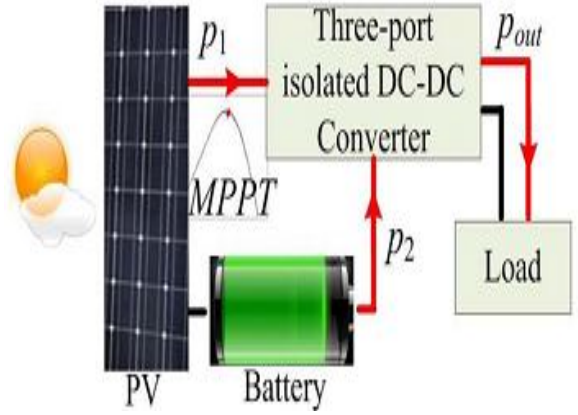

(b)

Fig. 5. Three working scenarios of the converter (the arrows show the directions of energy flow). (b) Scenario 2 (p1<pout): PV works in MPPT mode and battery works in discharge mode to provide the deficient energy. (c) Scenario 3 (p1=0): there is no solar energy available and battery is discharged to supply load.

Scenario 3 (p1=0): there is no solar power available and, thus, the battery is discharged to supply the load, as shown in Fig. 5(c). The active switches areS1andS3.

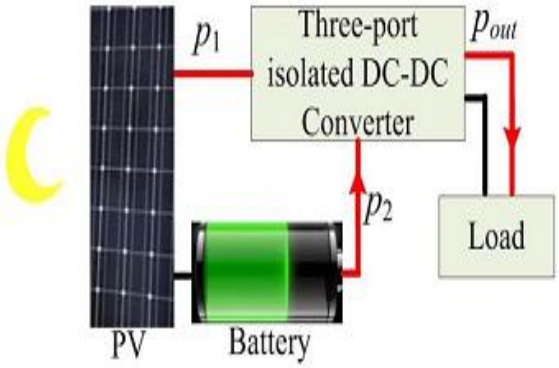

(c)

Fig. 5. Three working scenarios of the converter (the arrows show the directions of energy flow). (c) Scenario 3 (p1=0): there is no solar energy available and battery is discharged to supply load.

Fig. 6 shows the overall system with controllers, which include a MPPT controller for the PV panel and charge and discharge controllers for the battery.

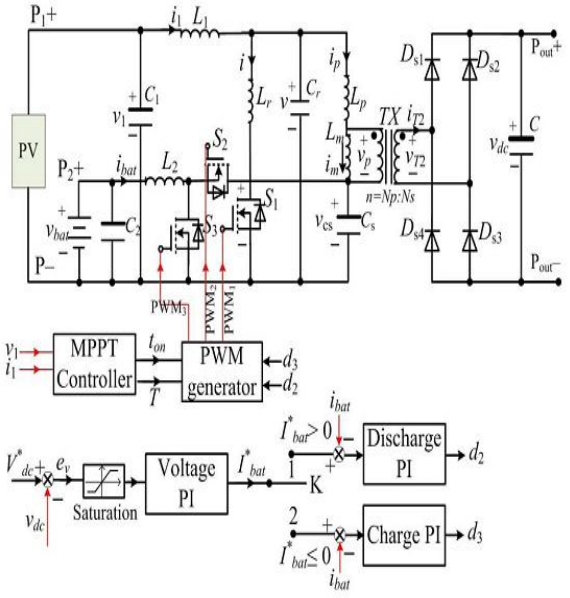

Fig. 6. Overall block diagram of the system with controllers.

B. MPPT Controller for PV Panel

The proposed converter is applied for MPPT control of a PV panel using the perturbation and observation (P&O) MPPT algorithm [21] to maximize the PV panel's output efficiency. Fig. 7 shows the flowchart of the MPPT algorithm.

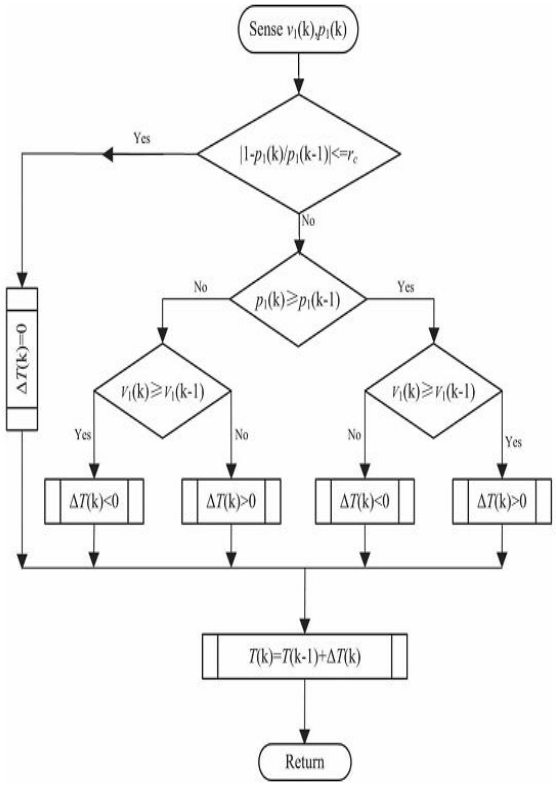

Fig. 7. Flowchart of the MPPT algorithm.

A ratio rc is defined to specify the relative power change (RPC) of the PV panel between two consecutive sampling steps. Thus,

$$r_c = \frac{|P_1(k)-P_1(k-1)|}{P_1(k-1)} \qquad (19)$$

Where P1(k)andP1(k−1)represent the measured output power of the PV panel in the kth and (k−1)th steps, respectively. As shown in Fig. 7, the P&O MPPT algorithm is realized by the frequency modulation method [2], where the conduction time ofS1, i.e., ton, is fixed so that S1can achieve soft switching.

C. Charge and Discharge Controllers for Battery

Fig. 8(a) and (b) shows the equivalent circuit of the battery and the converter when the battery works in the charge and discharge modes, respectively.

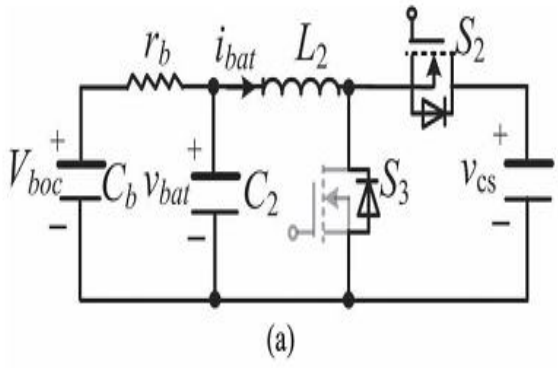

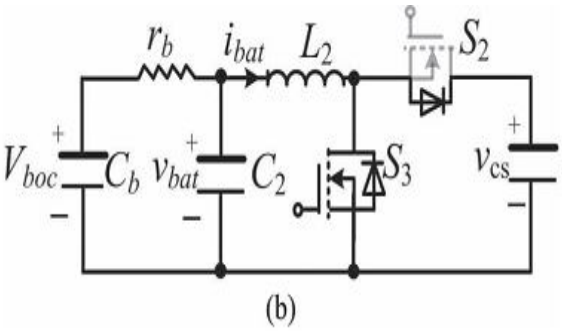

Fig. 8. Equivalent circuit of the battery with (a) the buck converter in charge mode and (b) the boost converter in discharge mode.

The bode plots of ibat(s)/d2(s)and ibat(s)/d3(s)without the PI compensations (i.e., the open-loop transfer functions) are shown in Fig. 9.

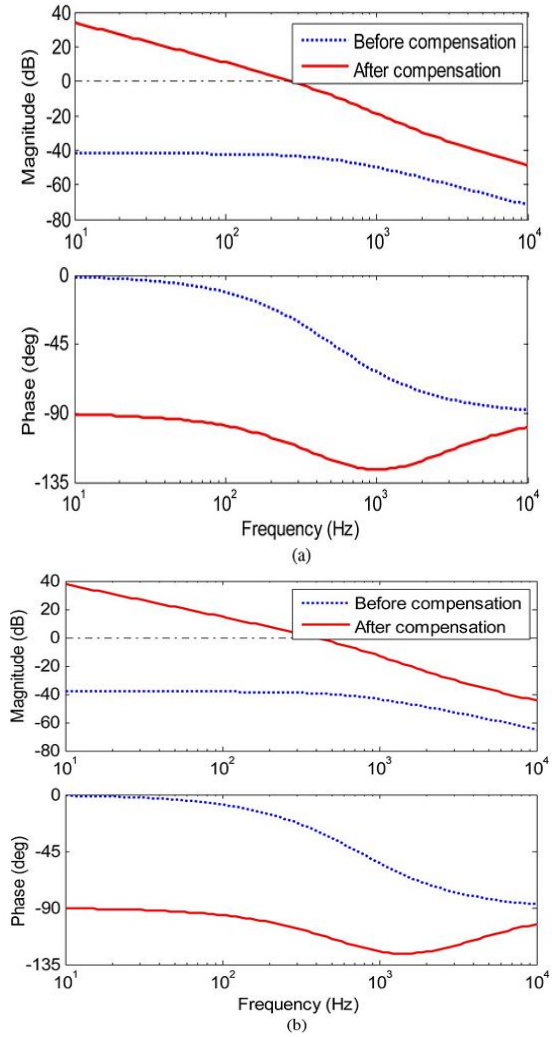

Fig. 9. Bode plots. (a)ibat(s)/d2(s).(b)ibat(s)/d3(s)

Once the current controllers are designed, the outer-loop dc link voltage controller, which has a lower cutoff frequency than the current loop, is then

designed. The PI parameters of the current and voltage controllers used in this paper are listed in Table I.

TABLE I: CONTROLLER PARAMETERS

	K_p	K_i
Current controller (charge)	2.5	5000
Current controller (discharge)	2.38	6600
Voltage controller	10	2

SIMULATION RESULTS

Simulations are carried in MATLAB/Simulink to validate the proposed converter and the controllers. The nominal voltage and internal resistance rb of the battery are 7.5 V and 0.16Ω, respectively.

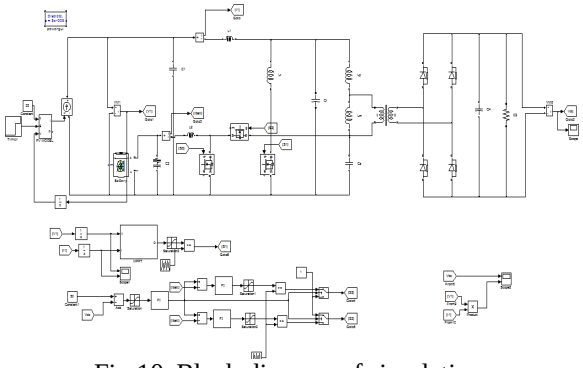

Fig.10. Block diagram of simulation

Fig. 11(a) shows that the initial solar radiation is zero and there is no power generated by the PV panel, as shown in Fig. 11(c). This indicates that the converter works in Scenario 1 and all of the power is supplied by discharging the battery. Fig. 11(b) shows that the dc-link voltage quickly reaches its reference value of 50 V.

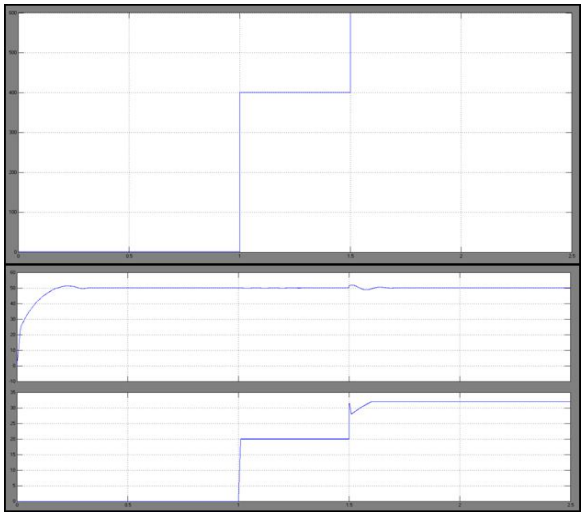

Fig. 11. Step responses: (a) profile of solar radiation, (b) dc-link voltage response, and (c) PV power response.

From 1 to 1.5 s, the converter works in Scenario 2. The PV panel generates the maximum power, as indicated in Fig. 11(c).

Fig. 12 shows the simulation results of the PV power and the dc-link voltage. As shown in Fig. 12(a), the energy extracted from the PV panel closely follows the ideal MPP by using the proposed converter and MPPT control algorithm. The dc-link voltage is well controlled at its desired value of 50 V.

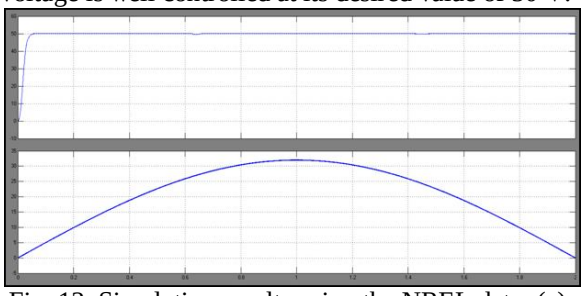

Fig. 12. Simulation results using the NREL data: (a) generated PV power and (b) the dc-link voltage.

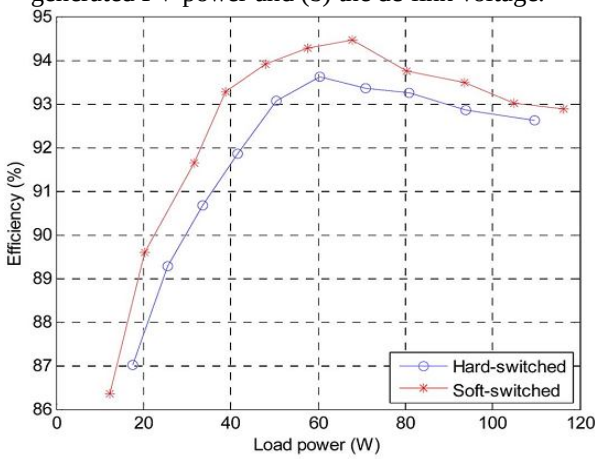

Fig. 13. Comparison of efficiency versus load power of the proposed soft switched converter and the hard-switched converter.

Fig. 13 compares the measured efficiencies of the proposed soft-switched converter and the hard-switched converter. The proposed soft-switched converter always has a higher efficiency than the hard-switched converter and has achieved the peak efficiency of 94.5%.

CONCLUSION

This paper proposed a new isolated ,three port bidirectional DC-DC converter which uses very less number of switches and is used for simultaneous power management of multiple energy sources. A new isolated three-port bidirectional dc–dc converter is proposed in this paper which uses the minimum number of switches. The proposed converter has been used for simultaneous power management of multiple energy sources, i.e., a PV panel and a battery. Simulation results have shown that the converter is not only capable of MPPT for the PV panel when

there is solar radiation but also can control the charge/discharge of the battery to maintain the dc-link voltage at a constant value. The proposed converter is applicable to other types of renewable energy sources, such as wind turbine generators. The main objective is to regulate the output DC link voltage to a constant value and also to manage the power for the sources. By using the simulation results we can analyze the proposed method.

REFERENCES

[1] C. Onwuchekwa and A. Kwasinski, "A modified-time-sharing switching technique for multiple-input DC-DC converters," IEEE Trans. Power Electron., vol. 27, no. 11, pp. 4492–4502, Nov. 2012.

[2] A. Khaligh, J. Cao, and Y. Lee, "A multiple-input DC-DC converter topology," IEEE Trans. Power Electron., vol. 24, no. 4, pp. 862–868, Mar. 2009.

[3] J. Lee, B. Min, D. Yoo, R. Kim, and J. Yoo, "A new topology for PV DC/DC converter with high efficiency under wide load range," inProc. Eur. Conf. Power Electron. Appl., Sep. 2007, pp. 1–6.

[4] C. Lohmeier, J. Zeng, W. Qiao, L. Qu, and J. Hudgins, "A currentsensorless MPPT quasi-double-boost converter for PV systems," inProc. IEEE Energy Convers. Congr. Expo., Sep. 2011, pp. 1069–1075.

[5] K. Sayed, M. Abdel-Salam, A. Ahmed, and M. Ahmed, "New high voltage gain dual-boost DC-DC converter for photovoltaic power system," Elect. Power Compon. Syst., vol. 40, no. 7, pp. 711–728, Apr. 2012.

[6] Y. Chen, Y. Liu, and F. Wu, "Multi-input DC/DC converter based on the multi winding transformer for renewable energy applications," IEEE Trans. Ind. Appl., vol. 38, no. 4, pp. 1096–1104, Jul./Aug. 2002.

[7] Y. Jang and M. Jovanovic, "Isolated boost converter,"IEEE Trans. Power Electron., vol. 22, no. 4, pp. 1514–1521, Jul. 2007.

[8] E. Yang, Y. Jiang, G. Hua, and F. Lee, "Isolated boost circuit for power factor correction," in Proc. IEEE Appl. Power Electron. Conf. Expo., Mar. 1993, pp. 196–203.

[9] Y. Lembeye, V. Bang, G. Lefevre, and J. Ferrieux, "Novel half-bridge inductive DC-DC isolated converters for fuel cell applications," IEEE Trans. Energy Convers., vol. 24, no. 1, pp. 203–210, Mar. 2009.

[10] J. Zeng, W. Qiao, L. Qu, and Y. Jiao, "An isolated multiport dc-dc converter for simultaneous power management of multiple different renewable energy sources,"IEEE J. Emerging Sel. Topics Power Electron., vol. 2, no. 1, pp. 70–78, Mar. 2014.

[11] H. Tao, A. Kotsopoulos, J. Duarte, and M. Hendrix, "Family of multiport bidirectional DC-DC converters,"Proc. Inst. Elect. Eng.—Elect. Power Appl., vol. 153, no. 3, pp. 451–458, May 2006.

[12] C. Zhao, S. Round, and J. Kolar, "An isolated three-port bidirectional DC-DC converter with decoupled power flow management," IEEE Trans. Power Electron., vol. 23, no. 5, pp. 2443–2453, Sep. 2008.